Does Chemistry Really Matter in the Chemical Vapor Deposition of Titanium Dioxide? Precursor and Kinetic Effects on the Microstructure of Polycrystalline Films

Charles J. Taylor,[†] David C. Gilmer,[†] Daniel G. Colombo,[†] G. D. Wilk,[‡] Stephen A. Campbell,[§] Jeff Roberts,*[,†] and Wayne L. Gladfelter*[,†]

Contribution from the Departments of Chemistry and Electrical Engineering, University of Minnesota, Minneapolis, Minnesota 55455, and Central Research Laboratory, Texas Instruments, Dallas, Texas 75243

Received December 28, 1998

Abstract: A side-by-side comparison of the TiO_2 deposition kinetics and the corresponding microstructures was studied. The two precursors were titanium(IV) isopropoxide and anhydrous titanium(IV) nitrate, and all depositions were conducted at low pressures ($<10^{-4}$ Torr) in an ultrahigh vacuum chemical vapor deposition reactor. For both precursors deposition kinetics were qualitatively similar and exhibited three distinct regimes as a function of temperature. At the lowest temperatures, growth was limited by the rate of precursor reaction on the substrate surface. At intermediate temperatures flux-limited growth was obtained, and at the highest temperatures the growth rates decreased with increasing temperatures. The overall behavior was modeled quantitatively for each precursor using a two-step mechanism involving reversible adsorption followed by irreversible reaction. Titanium(IV) nitrate exhibited a lower activation energy of reaction ($E_r = 98$ kJ/mol) which allowed deposition at lower temperatures compared to titanium(IV) isopropoxide ($E_r = 135$ kJ/mol). The film microstructures were examined using transmission and scanning electron microscopy and X-ray diffraction. Comparison of the microstructures of films deposited at similar temperatures revealed significant differences in the reaction rate-limited regime. As the growth rates of the two precursors converged in the flux-limited regime, the respective microstructures became indistinguishable. The importance of precursor surface coverage and diffusion on this effect is described.

Introduction

The composition and structure (including microstructure) of a solid-state material determine its properties. Factors that control composition and structure become of obvious importance for preparing solids with desirable properties. In chemical vapor deposition (CVD) processes, molecular precursors must shed the ligands that contributed to their volatility in order to produce a film of a solid-state material. The question posed in the title is of fundamental and technological interest in the CVD of TiO_2, and the same question can be asked for all CVD processes.

Titanium dioxide is a candidate to replace SiO_2 as the gate dielectric in metal oxide semiconductor field effect transistors (MOSFETs).[1−3] The continuing decrease in device dimensions requires the thickness of the gate oxide to shrink. Ultimately, the SiO_2 gate thickness will reach a value (approximately 15−20 Å) at which direct electron tunneling through the SiO_2 layer raises the leakage current to unacceptable levels. One solution to this problem would be to replace the SiO_2 layer with another material of higher dielectric constant. This would achieve an equivalent capacitance using a thicker layer, thereby reducing leakage current. Titanium dioxide,[1−3] Ta_2O_5,[4,5] various perovskites ($Ba_xSr_{1-x}TiO_3$, etc.),[6−9] and mixed-metal oxides ($Ti_xZr_ySn_zO_2$)[10] are candidates under consideration for this application. The two primary figures of merit for this application, dielectric constant and leakage current, are critically dependent on the composition and microstructure of the metal oxide films and the interfacial region between metal oxide and silicon.

The chemical vapor deposition of titanium dioxide has been practiced for over four decades.[1−3,11−37] The most commonly

[†] Department of Chemistry, University of Minnesota.
[‡] Texas Instruments.
[§] Department of Electrical Engineering, University of Minnesota.

(1) Yan, J.; Gilmer, D. C.; Campbell, S. A.; Gladfelter, W. L.; Schmid, P. G. *J. Vac. Sci. Technol., B* **1996**, *14*, 1706.
(2) Campbell, S. A.; Gilmer, D. C.; Wang, X.-C.; Hsieh, M.-T.; Kim, H.-S.; Gladfelter, W. L.; Yan, J. *IEEE Trans. Electron Devices* **1997**, *44*, 104.
(3) Gilmer, D. C.; Colombo, D. G.; Taylor, C. J.; Roberts, J.; Haugstad, G.; Campbell, S. A.; Kim, H.-S.; Wilk, G. D.; Gribelyuk, M. A.; Gladfelter, W. L. *Chem. Vap. Deposition* **1998**, *4*, 9.
(4) Treichel, H.; Mitwalsky, A.; Tempel, G.; Zorn, G.; Bohling, D. A.; Coyle, K. R.; Felker, B. S.; George, M.; Kern, W.; Lane, A. P.; Sandler, N. P. *Adv. Mater. Opt. Electron.* **1995**, *5*, 163.
(5) Son, K.-A.; Mao, A. Y.; Kim, B. Y.; Liu, F.; Pylant, E. D.; Hess, D. A.; White, J. M.; Kwong, D. L.; Roberts, D. A.; Vrtis, R. N. *J. Vac. Sci. Technol., A* **1998**, *16*, 1670.
(6) Arita, K.; Fujii, E.; Shimada, Y.; Uemoto, Y.; Nasu, T.; Inoue, A.; Matsuda, A.; Otsuki, T.; Suzuoka, N. *Jpn. J. Appl. Phys.* **1994**, *33*, 5397.
(7) Gilbert, S. R.; Wessels, B. W.; Neumayer, D. A.; Marks, T. J.; Schindler, J. L.; Kannewurf, C. R. In *Metal-Organic Chemical Vapor Deposition of Electronic Ceramics*; Desu, S. B., Beach, D. B., Wessels, B. W., Gokoglu, S., Eds.; Materials Research Society: Pittsburgh, 1994; Vol. 41.
(8) Kawahara, T.; Yamamuka, M.; Makita, T.; Naka, J.; Yuuki, A.; Mikami, N.; Ono, K. *Jpn. J. Appl. Phys.* **1994**, *33*, 5129.
(9) Kuroiya, T.; Tsunemine, Y.; Horikawa, T.; Makita, T.; Tanimura, J.; Mikami, N.; Sato, K. *Jpn. J. Appl. Phys.* **1994**, *33*, 5187.
(10) van Dover: R. B.; Schneemeyer, L. F.; Fleming, R. M. *Nature* **1998**, *392*, 162.
(11) Hass, G. *Vacuum* **1952**, *2*, 331.
(12) Feuersanger, A. E. *Proc. IEEE* **1964**, *52*, 1463.
(13) Ghoshtagore, R. N.; Norieka, A. J. *J. Electrochem. Soc.* **1970**, *117*, 1310.
(14) Ghoshtagore, R. N. *J. Electrochem. Soc.* **1970**, *117*, 529.
(15) Fitzgibbons, E. T.; Sladek, K. J.; Hartwig, W. H. *J. Electrochem. Soc.* **1972**, *119*, 735.

10.1021/ja984446f CCC: $18.00
Published on Web 05/22/1999

used precursor, titanium(IV) isopropoxide (TTIP), can be directly thermolyzed (eqs 1 and 2) or hydrolyzed (eq 3) to produce TiO_2.

$$Ti(O\text{-}i\text{-}Pr)_4 \rightarrow TiO_2 + 4H_3C{-}CH{=}CH_2 + 2H_2O \quad (1)$$

$$Ti(O\text{-}i\text{-}Pr)_4 \rightarrow TiO_2 + 2H_3C{-}CH{=}CH_2 + 2HO\text{-}i\text{-}Pr \quad (2)$$

$$Ti(O\text{-}i\text{-}Pr)_4 + 2H_2O \rightarrow TiO_2 + 4HO\text{-}i\text{-}Pr \quad (3)$$

Other precursors include $TiCl_4$ (which requires O_2 or H_2O as a reactant).[13,14] Although not required by reaction stoichiometries shown in eqs 1 and 2, oxygen or another strong oxidant (e.g., N_2O)[32] is often added to the deposition system to increase the rate of deposition and/or the quality of the film. To bypass the need for the addition of water or an oxidant to the deposition, we examined the use of titanium(IV) nitrate (TN) for the growth of TiO_2 films.

Low-pressure and ultrahigh vacuum chemical vapor depositions (LPCVD and UHV-CVD, respectively) of crystalline TiO_2 using TN were accomplished at temperatures as low as 159 °C.[3] Following postdeposition annealing, capacitors (with 30−35 nm thick TiO_2 films) constructed with Pt gate electrodes exhibited dielectric constants in the range of 19−30 and leakage current densities as low as 10^{-8} A/cm^2. These results were comparable to those achieved for TiO_2 films grown using TTIP. More recent results, however, have suggested that capacitors prepared using TN-grown films exhibit higher dielectric constants and lower leakage currents.

In this paper we compare the growth of TiO_2 films using TN and TTIP under nearly identical conditions in a UHV-CVD reactor. The molecular structure of TN (shown below) is based on a single-crystal X-ray diffraction study.[38] The structure of TTIP, however, is a volatile liquid at room temperature and is assumed to be monomeric. The change in microstructures (crystallinity, texture, grain size, and shape) over a wide range of deposition temperatures correlates with the deposition kinetics.

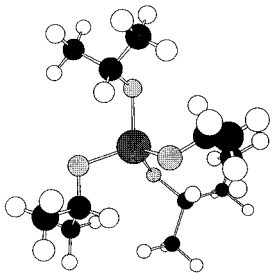

$Ti(OC_3H_7)_4$ (TTIP)

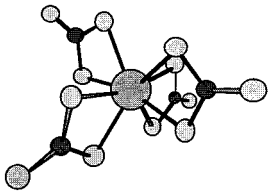

$Ti(NO_3)_4$ (TN)

Experimental Section

Titanium dioxide films were deposited by chemical vapor deposition in a UHV-compatible reactor.[30] The typical base pressure prior to a deposition was 5×10^{-9} Torr. The precursor vessels were constructed of Pyrex glass tubes with glass-to-metal junctions connected to VCR fittings and sealed with stainless steel bonnet valves. Precursors were heated to 50−60 °C to increase their volatility, and the transfer lines were heated to 58 °C to prevent precursor condensation in the lines. The precursor flux was controlled using a UHV-compatible variable leak valve through a 0.5 in. o.d. dosing tube. The growth substrate for all experiments was Si(100). Substrates were (a) dipped in 4:1 H_2SO_4/H_2O_2 to remove any organic contaminants, (b) rinsed with deionized water and blown dry with N_2, (c) dipped in 5% HF for several seconds to prepare the H-terminated surface, and (d) rinsed with deionized water and blown dry with N_2. Samples were immediately mounted on a molybdenum disk and transferred into the reactor via a load-lock chamber pumped with a turbomolecular pump. Under UHV conditions, electron bombardment on the back of the Mo disk heated the substrates to ≥800 °C to desorb hydrogen, which was evident by a pressure increase around 700 °C. Reflection high-energy electron diffraction verified that this thermal treatment produced an ordered Si(100)2×1 surface. The substrate was then cooled to the desired deposition temperature, which was kept constant throughout the deposition by maintaining a constant power to the e-beam heater. Temperatures were measured using an optical pyrometer (E2T Pulsar II or Everest 430AH). The reactor pressure was monitored throughout the depositions using an ion gauge (Granville-Philips 271).

Deposition experiments were performed in the absence of carrier gas with precursor pressures in the range 5×10^{-6} to 8×10^{-5} Torr. Deposition times ranged from 20 min to 7 h, and film thicknesses ranged from 12 to 430 nm. Films were characterized by X-ray diffraction (Siemans D-5005), Rutherford back-scattering (RBS), and scanning electron microscopy (SEM) (Hitachi S-900). Selected samples were also examined with high-resolution transmission electron microscopy (TEM). Film thicknesses were measured by cross-sectional SEM and ellipsometry. In general, films deposited by both precursors exhibited good adhesion to the substrate and were uniform in appearance.

Results

Deposition Kinetics. The TiO_2 growth kinetics from TTIP and TN were evaluated in the temperature range 159−890 °C. Thicknesses of the films were determined using cross-sectional SEM and/or ellipsometry and were converted into growth rates. Film densities were determined by comparing the RBS-measured thickness (modeled assuming the theoretical density of anatase or rutile) to the thickness measured by cross-sectional SEM. For all films, the densities were approximately 80% of the corresponding single-crystal values.

No attempt was made to separate nucleation from steady-state growth in these measurements, and the values therefore

(16) Balog, M.; Schieber, M.; Patai, S.; Michman, M. *J. Cryst. Growth* **1972**, *17*, 298.
(17) Takahashi, Y.; Tsuda, K.; Sugiyama, K.; Minoura, H.; Makino, D.; Tsuiki, M. *J. Chem. Soc., Faraday Trans. 1* **1981**, *77*, 1051.
(18) Fuyuki, T.; Matsunami, H. *Jpn. J. Appl. Phys.* **1986**, *25*, 1288.
(19) Fuyuki, T.; Kobayashi, T.; Matsnami, H. *J. Electrochem. Soc.* **1988**, *135*, 248.
(20) Kamata, K.; Maruyama, K.; Amano, S.; Fukazawa, H. *J. Mater. Sci. Lett.* **1990**, *9*, 316.
(21) Lu, J.; Raj, R. *J. Mater. Res.* **1991**, *6*, 1913.
(22) Chang, H. L. M.; You, H.; Guo, J.; Lam, D. J. *Appl. Surf. Sci.* **1991**, *48/49*, 12.
(23) Lakomaa, E.-L.; Haukka, S.; Suntola, T. *Appl. Surf. Sci.* **1992**, *60/61*, 742.
(24) Won, T.; Yoon, S.; Kim, H. *J. Electrochem. Soc.* **1992**, *139*, 3284.
(25) Chang, H. L. M.; You, H.; Gao, Y.; Guo, J.; Foster, C. M.; Chiarello, R. P.; Zhang, T. J.; Lam, D. J. *J. Mater. Res.* **1992**, *7*, 2495.
(26) Ritala, M.; Leskelä, M.; Nykänen, E.; Soininen, P.; Niinistö, L. *Thin Solid Films* **1993**, *225*, 288.
(27) Wu, Y.; Bradley, D. C.; Nix, R. M. *Appl. Surf. Sci.* **1993**, *64*, 21.
(28) Ritala, M.; Leskelä, M.; Niinistö, L.; Haussalo, P. *Chem. Mater.* **1993**, *5*, 1174.
(29) Rausch, N.; Burte, E. P. *J. Electrochem. Soc.* **1993**, *140*, 145.
(30) Chen, S.; Masen, M. G.; Gysling, H. J.; Paz-Pujalt, G. R.; Blanton, T. N.; Castro, T.; Chen, K. M.; Fictorie, C. P.; Gladfelter, W. L.; Franciosi, A.; Cohen, P. I.; Evans, J. F. *J. Vac. Sci. Technol., A* **1993**, *11*, 2419.
(31) Chang, H. L. M.; Zhang, T. J.; Zhang, H.; Guo, J.; Kim, H. K.; Lam, D. J. *J. Mater. Res.* **1993**, *8*, 2634.
(32) Yoon, Y. S.; Kang, W. N.; Yom, S. S.; Kim, T. W.; Jung, M.; Park, T. H.; Seo, K. Y.; Lee, J. Y. *Thin Solid Films* **1994**, *238*, 12.
(33) Kim, T. W.; Jung, M.; Kim, H. J.; Park, T. H.; Yoon, Y. S.; Kang, W. N.; Yom, S. S.; Na, H. K. *Appl. Phys. Lett.* **1994**, *64*, 1407.
(34) Fictorie, C. P.; Evans, J. F.; Gladfelter, W. L. *J. Vac. Sci. Technol., A* **1994**, *12*, 1108.
(35) Aarik, J.; Aidla, A.; Uustare, T.; Sammelselg, V. *J. Cryst. Growth* **1995**, *148*, 268.
(36) Versteeg, V. A.; Avedisian, T. C.; Raj, R. *J. Am. Ceram. Soc.* **1995**, *78*, 2763.
(37) Zhang, Q.; Griffin, G. L. *Thin Solid Films* **1995**, *263*, 65.
(38) Garner, C. D.; Wallwork, S. C. *J. Chem. Soc. A* **1966**, 1496.

Table 1. Summary of Kinetic Data

precursor	temp, °C	pressure, 10^{-6} Torr	time, min	thickness, nm	rate, nm/min	phase
TTIP	500	10	77	94.3	1.22	A
TTIP	500	20	38	99.8	2.63	A
TTIP	500	40	22.5	98.0	4.36	A
TTIP	500	80	15	109	7.24	A
TN	420	5.4	120	100	0.83	A
TN	420	8	90	103	1.15	A
TN	420	11	80	136	1.69	A
TN	420	24	60	187	3.12	A
TN	420	30	46	190	4.14	A
TTIP	323	40	435	66.2	0.15	A
TTIP	352	40	165	64.3	0.34	A
TTIP	367	40	105	66.0	0.63	A
TTIP	370	40	100	80	0.80	A
TTIP	390	40	55	55.4	1.01	A
TTIP	396	40	45	67.5	1.50	A
TTIP	480	40	29	91.5	3.15	A
TTIP	580	40	30	98.8	3.29	A
TTIP	700	40	30	251	2.79	A/R
TTIP	845	40	42	143	1.91	R
TTIP	920	40	60	69	1.16	R
TN	159	18	420	170	0.33	A
TN	184	18	135	150	1.04	A
TN	208	18	75	185	2.47	A
TN	220	18	60	200	3.33	A
TN	230	18	25	120	4.80	A
TN	250	18	35	200	5.71	A
TN	525	18	10	55	5.50	A
TN	550	18	6	33	5.50	A
TN	560	18	4	20	5.00	A
TN	700	18	90	360	4.00	A/R
TN	800	18	4	12	3.00	R
TN	890	18	55	140	2.55	R
TN	900	18	120	200	1.67	R

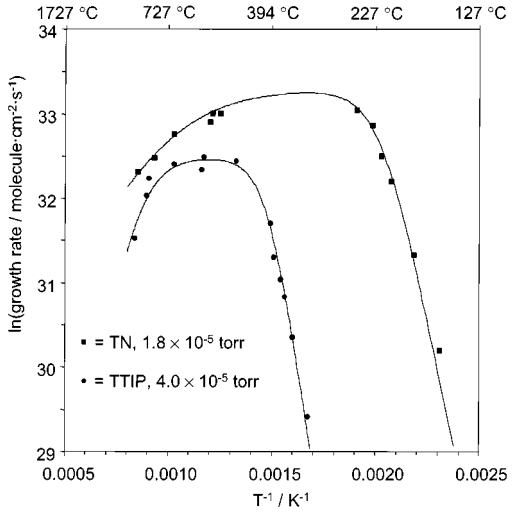

Figure 1. Temperature dependence of the growth rate. The individual data points are from the experimental measurements, and the solid lines are derived from the model discussed in the text.

represent average growth rates over the entire deposition period. Preliminary measurements suggest, however, that the induction period was always a small fraction of the deposition period. The kinetic data are summarized in Table 1, and the temperature dependence of the growth is plotted in Figure 1. For the experiments represented in Figure 1, the TTIP partial pressure was 4.0×10^{-5} Torr, and the TN partial pressure was 1.8×10^{-5} Torr. For both of the precursors, the deposition kinetics follow apparent Arrhenius behavior at low temperatures (<∼250 °C for TN and <∼400 °C for TTIP). At intermediate deposition temperatures (400−700 °C for TTIP and 250−600 °C for TN),

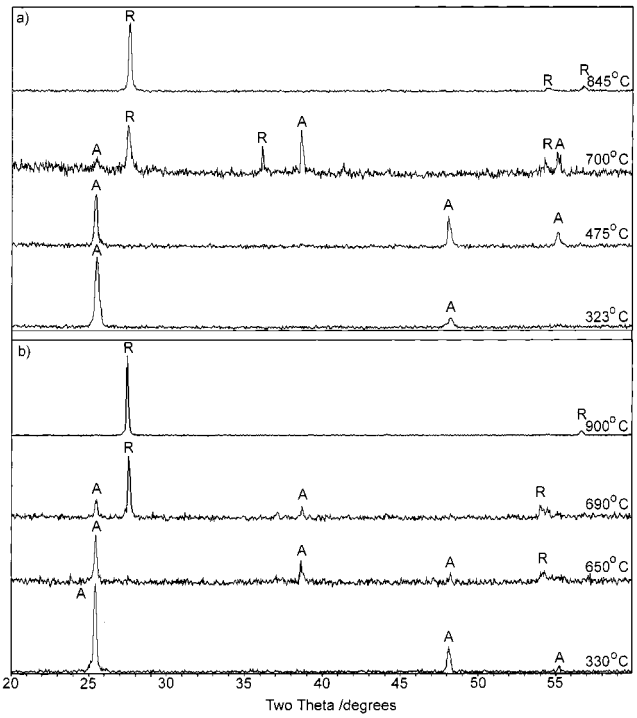

Figure 2. XRD of the TiO_2 films deposited using (a) TTIP and (b) TN at different temperatures showing the crossover from anatase to rutile films. The 2Θ values of the anatase reflections and their assignments are 25.49 (101), 38.60 (112), 48.25 (200), and 55.10 (211). The observed rutile reflections and their assignments are 27.59 (110), 54.59 (211), and 56.76 (220).

the TiO_2 growth rate is independent of substrate temperature, suggesting that deposition is flux-limited. In this regime, pressure dependence measurements (Table 1) demonstrated that growth is first order in precursor pressure. It is important to point out that the precursor reaction probability need not be unity or even near unity in the flux-limited regime. For the indicated pressures (4.0×10^{-5} Torr for TTIP, 1.8×10^{-5} Torr for TN), the flux-limited growth rates are 33 and 55 Å·min^{-1}, respectively. Assuming that the films have a density that is 80% that of anatase ($\rho_{anatase} = 3.90$ g·cm^{-3}), these linear growth rates correspond to mass accumulation rates of 1.0×10^{-7} g·cm^{-2}·s^{-1} for TTIP and 1.7×10^{-7} g·cm^{-2}·s^{-1} for TN. These numbers in turn imply precursor reaction probabilities of 0.0029 for TTIP and 0.012 for TN. Such low reaction probabilities are not unprecedented. In earlier work on aluminum CVD from dimethylethylamine alane, the precursor reaction probability in the flux-limited regime was shown to be 0.13.[39] At high temperatures (>700 °C for TTIP and >600 °C for TN), the TiO_2 growth rate decreases with increasing temperature.

Microstructure. In the temperature and pressure ranges explored in this UHV-CVD study (Table 1), films from both precursors progress from polycrystalline anatase films below approximately 650 °C to polycrystalline rutile films above 700 °C (Figure 2). X-ray diffraction patterns exhibited line widths at all temperatures characteristic of coherent lengths >10 nm.

The most significant difference between the microstructures of the two types of TiO_2 films occurs in the lower temperature regime where the films are largely polycrystalline anatase. Plan-view (Figure 3) and cross-sectional SEM images of films deposited from TTIP at 323 °C establish that the films are composed of approximately equidimensional grains extending

(39) Karpov, I.; Gladfelter, W. L.; Franciosi, A. *Appl. Phys. Lett.* **1996**, *69*, 4191.

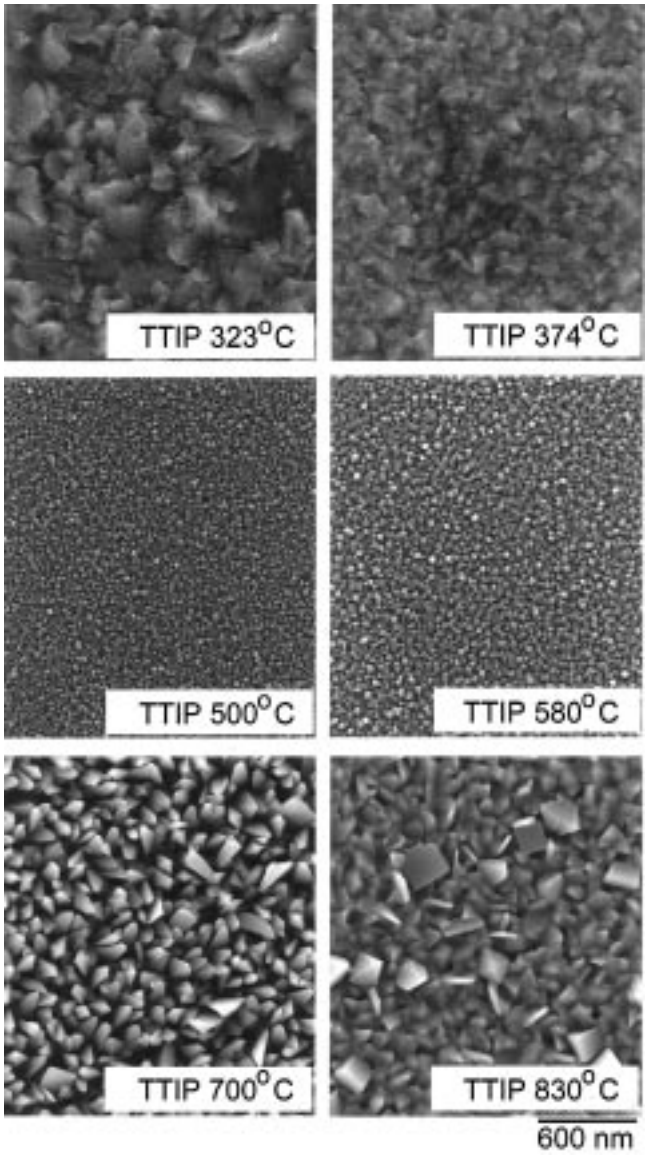

Figure 3. Plan-view SEM of TTIP-deposited TiO_2 at different temperatures. The scale for all of the photographs is shown in the lower right-hand corner. The thicknesses of the films in order of increasing temperature are 66, 70, 70, 99, 250, and 190 nm.

the entire depth of the film and exhibiting fully developed facets at the air interface. Viewed from above, the average grain width is 200−300 nm. A summary of the grain size as a function of temperature is located in Table 2. As the deposition temperature increases, the mean grain width decreases. The majority of the grains continue to extend to the substrate, leading to a well-developed columnar microstructure. At 390 °C the average cross-sectional area of individual grains is 0.0047 μm^2. The columns are roughly perpendicular to the substrate (Figure 4). The trend of decreasing grain size continues at 500 °C where the columns of TiO_2 are only 30 nm wide (cross-sectional area 0.0011 μm^2). At higher temperatures the columnar microstructure remains, but the width of the columns has increased. The plan-view SEM of the film grown at 830 °C displays evidence of coalescence between adjacent grains consistent with more extensive sintering of the TiO_2.

Figure 5 shows the temperature-dependent microstructure of polycrystalline TiO_2 films grown using TN. At the lowest temperature (159 °C, not shown in the figure), large grains appear and eventually cover the entire substrate. As the deposition temperature increases to 250 °C, the large grains seem

Table 2. Grain Size Analysis

precursor	temp, °C	film thickness, nm	no. of grains measd	av grain size, μm^2
TTIP	323	66	15	0.06930 ± 0.0260
TTIP	374	70	71	0.02630 ± 0.0096
TTIP	390	55	79	0.00473 ± 0.0014
TTIP	500	75	14	0.00112 ± 0.0002
TTIP	580	99	13	0.00172 ± 0.0005
TTIP	700	250	66	0.00784 ± 0.0034
TTIP	830	19	74	0.01540 ± 0.0105
TN	220	200	10	0.31900 ± 0.1304
TN	330	380	117	0.10110 ± 0.0578
TN	525	55	16	0.00048 ± 0.0001
TN	550	22	16	0.00084 ± 0.0003
TN	643	40−60	105	0.00391 ± 0.0022
TN	700	360	59	0.00609 ± 0.0025
TN	890	140	84	0.01956 ± 0.0107
TN	900	200	59	0.03246 ± 0.0220

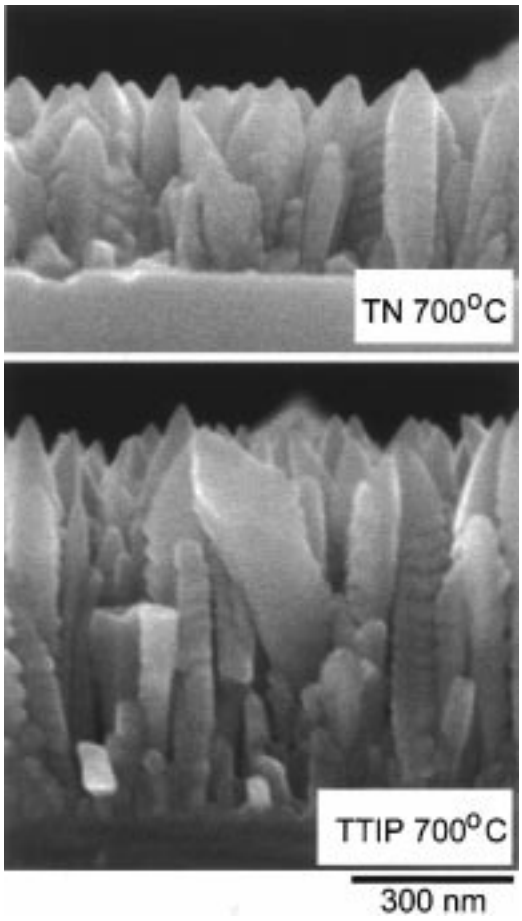

Figure 4. Cross-sectional SEM of polycrystalline TiO_2 films grown at 700 °C using TTIP and TN.

to fragment along a particular crystallographic direction. At higher temperatures (300−400 °C) the fragmentation becomes so pronounced that the original subgrain structure evolves into a set of smaller grains, all apparently with an orientation related to that of the larger domain. The crystal chemistry involved in this fascinating transformation is the subject of continuing study. By 500 °C, the TiO_2 films produced from TN exhibit a columnar microstructure (Figure 4), and *they are virtually indistinguishable from films produced using TTIP at the same temperature*. At and above 800 °C, the columnar grains in all films increase in size and begin to coalesce.

All of the results described above refer to as-deposited films. To probe the stability of the microstructure, individual TiO_2

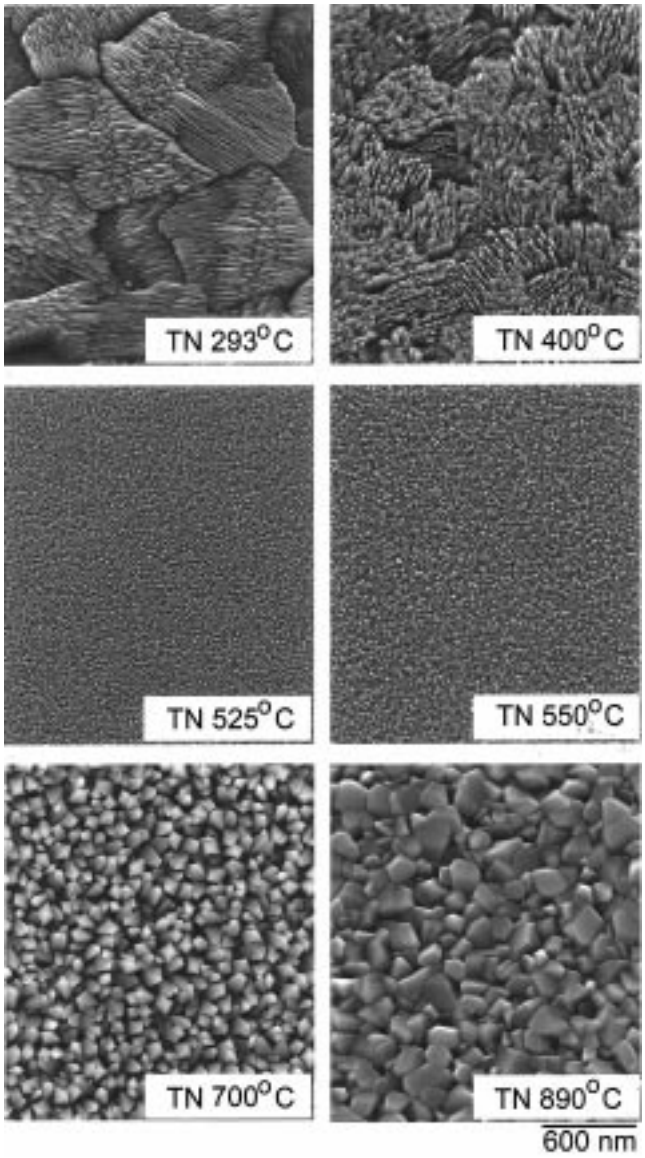

Figure 5. Plan-view SEM of TN-deposited TiO_2 at different temperatures. The scale for all of the photographs is shown in the lower right-hand corner. The thicknesses of the films in order of increasing temperature are 27, 260, 55, 33, 37, and 140 nm. The grain sizes from the 293 and 400 °C micrographs shown in this figure were not determined and are not listed in Table 2.

films deposited using TTIP at 435 °C were heated under UHV conditions for 12−18 min at temperatures ranging from 740 to 880 °C. Only at the highest temperature did noticeable sintering occur on this time scale. Those samples heated above 780 °C transformed from anatase to rutile.

Cross-Deposition Studies. Deposition of a 30 nm TiO_2 film using TN at 330 °C was followed by growth of an additional 40 nm film using TTIP at 360 °C. The specific temperatures were chosen to allow comparison to films grown at the same temperature for a given precursor. As can be seen in Figure 6, the microstructure of the resulting film is almost indistinguishable from the films grown only using TTIP. The average grain size estimated from the plan-view SEM is $0.045 \pm 0.017\ \mu m^2$, which is slightly larger than the average found for films grown exclusively from TTIP ($0.026 \pm 0.009\ \mu m^2$).

The analogous experiment starting with TTIP-deposited TiO_2 at 374 °C (30 nm) followed by TN-grown material (120 nm at 330 °C) results in films resembling those grown only from TN at the same temperature (Figure 6). To quantify and compare grain size for these films, we define a grain as the larger domain of similarly oriented subgrains. The average grain size estimated from the plan-view SEM is $0.025 \pm 0.013\ \mu m^2$, which agrees with the average found for films grown exclusively from TTIP ($0.026 \pm 0.010\ \mu m^2$) at the same temperature.

The Si/TiO_2 Interface. Another feature common to both precursors is the formation of a thin amorphous layer of material directly on the silicon substrate. Cross-sectional TEMs of films derived from both precursors are shown in Figure 7. Because the layer is so thin (<20 Å), direct determination of the precise composition is difficult and has not been accomplished. On the basis of electrical measurements obtained from capacitors constructed using the TiO_2 films,[1,40] we infer that the interfacial layer has a significantly lower dielectric constant than that of pure TiO_2 films. The most likely candidate is a mixture of Ti and Si oxides. Other researchers have reported the formation of an oxide layer of similar thickness resulting from the deposition of metal oxides on silicon.[29,32] Annealing at 450 °C in an oxygen atmosphere causes the thickness of the interfacial layer to increase.[1,40]

Discussion

Deposition Kinetics. From the data in Figure 1, we identify three regimes of CVD growth: (i) a low-temperature regime (<250 °C for TN and <400 °C for TTIP) in which the TiO_2 deposition rate increases rapidly with temperature, (ii) an intermediate regime (250−600 and 400−700 °C for TN and TTIP, respectively) in which the deposition rate is roughly independent of temperature, and (iii) a high-temperature regime, for which the deposition rate decreases with increasing temperature. Similar growth rate trends have been reported for many other CVD systems. The low-temperature regime is usually attributed to *reaction-limited* deposition, i.e., to CVD growth, which is limited by the rate of precursor decomposition. The growth rate increases with temperature due to Arrhenius dependence on thermal energy. At intermediate temperatures, growth becomes limited by the precursor−substrate collision rate: a solid can grow no faster than the rate at which the gas-phase precursor is delivered to the growth surface. In this regime, growth is said to be *flux-limited*, and the growth rate is independent of temperature.

The origin of the high-temperature regimes in the present systems, in which the growth rates decrease with increasing temperature, could be due to several factors. Analogous observations in higher pressure CVD systems are often attributed to precursor loss through gas-phase decomposition,[41] but the high vacuum conditions employed in this work make such a process very unlikely. Stoichiometric analysis of the films confirms that they are TiO_2 over the entire deposition temperature range, so the decreased growth rate is probably not associated with the opening of a new, nonproductive precursor decomposition channel, especially since both TTIP and TN show qualitatively similar growth rate trends. RBS analysis demonstrates that films deposited at high temperatures are more dense than those deposited at low temperatures due to particle sintering and to the anatase → rutile phase transition. However, the density change between the lowest and highest temperatures investigated is ∼10%, whereas for both TN and TTIP the magnitude of the growth rate decrease between the flux-limited regime and the highest temperature studied is >50%. Clearly,

(40) Kim, H.-S.; Gilmer, D. C.; Campbell, S. A.; Polla, D. L. *Appl. Phys. Lett.* **1996**, *69*, 3860.

(41) Kodas, T. T.; Hampden-Smith, M. J. In *The Chemistry of Metal CVD*; Kodas, T. T., Hampden-Smith, M. J., Eds.; VCH Publishers: New York, 1994; Vol. 429.

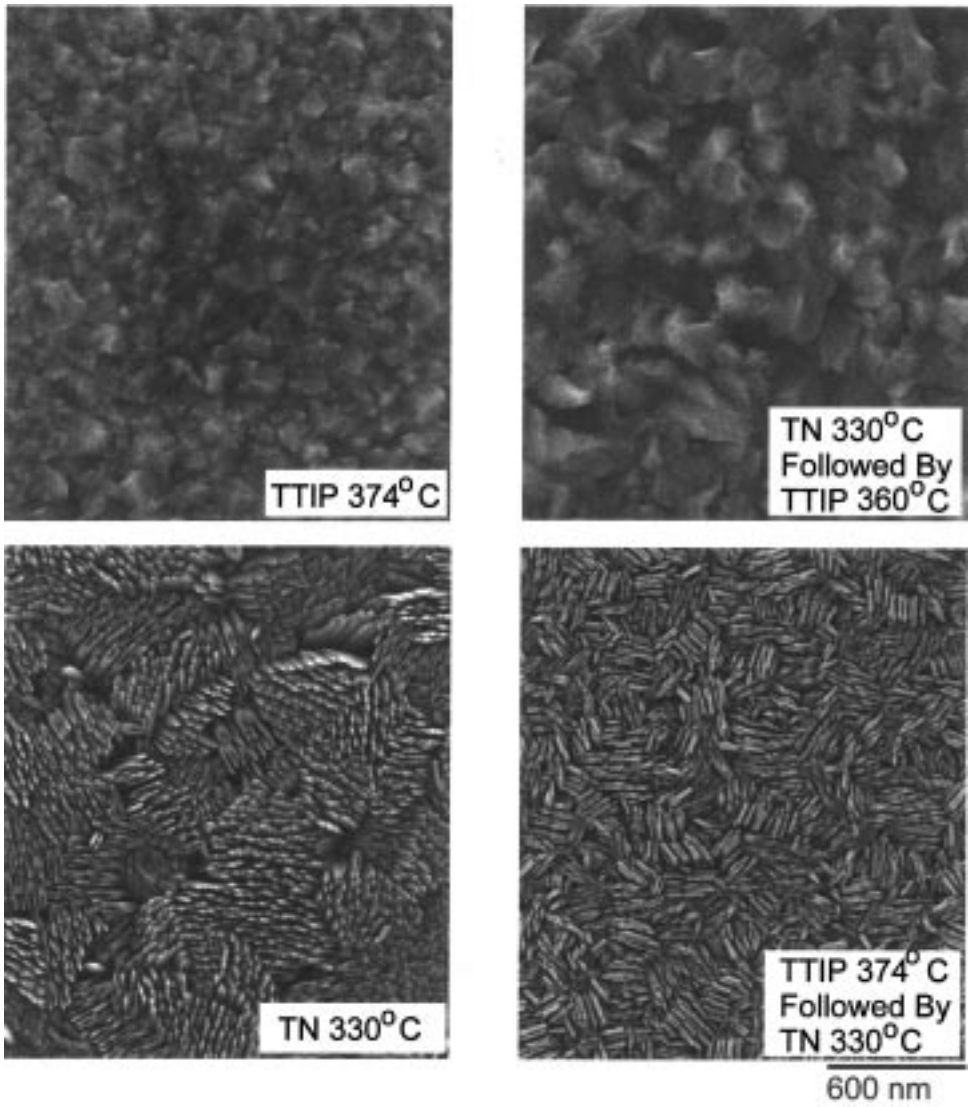

Figure 6. Plan-view SEM of TiO_2 films prepared in the cross-deposition studies. The scale for all of the photographs is shown in the lower right-hand corner. The thickness of the TTIP-deposited film (upper left) was 68 nm. In the TTIP on TN experiment (upper right), the TN-deposited layer was estimated to be 30 nm, and the subsequent TTIP-deposited layer was 40 nm. The TN-deposited film (lower left) was 380 nm. The underlying TTIP layer in the TN on TTIP experiment was 30 nm, and the subsequent TN-deposited layer was 120 nm. In the cross-deposition experiments, the thicknesses were based on known growth rates and the deposition times.

Scheme 1. Summary of the Kinetic Events Involved in the TiO_2 UHV-CVD

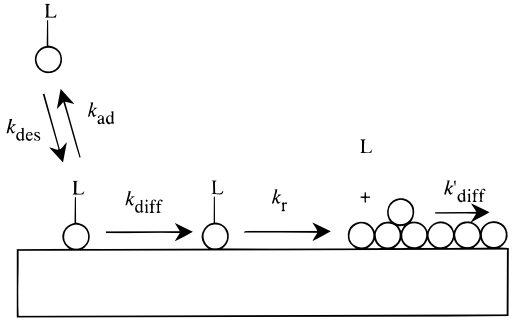

the decreasing growth rates at high temperatures are associated with another phenomenon.

The TiO_2 growth rate trends for both TTIP and TN can be rationalized by invoking rapid precursor desorption at high substrate temperatures. Scheme 1 summarizes the generic events involved in a UHV-CVD process. We analyze the growth kinetics in terms of a two-step model. The first step is reversible adsorption of the precursor (**P**) on the growth surface, and the second is irreversible reaction of adsorbed **P** to form solid TiO_2:

$$\mathbf{P}_{(g)} \underset{k_{des}}{\overset{k_{ad}}{\rightleftharpoons}} \mathbf{P}_{(ad)} \tag{4}$$

$$\mathbf{P}_{(ad)} \xrightarrow{k_r} TiO_{2(s)} + \text{byproducts}_{(g)} \tag{5}$$

where k_{ad}, k_{des}, and k_r are the rate constants for adsorption, desorption, and reaction, respectively. We emphasize that the precise nature of the chemisorbed precursor, $\mathbf{P}_{(ad)}$, is unknown. The rate of TiO_2 formation, R, is then given by

$$R = k_r \Theta_{\mathbf{P}} \tag{6}$$

where $\Theta_{\mathbf{P}}$ is the coverage of adsorbed precursor. Once a continuous TiO_2 film is formed on the growth substrate, CVD growth is in a steady state, where R does not change with time, provided that the temperature and precursor pressure are held constant. If dR/dt is zero, then so is $d\Theta_{\mathbf{P}}/dt$; that is, the rates of formation and disappearance of adsorbed **P** are exactly equal. The rate of formation of $\mathbf{P}_{(ad)}$ is simply the product of the gas−

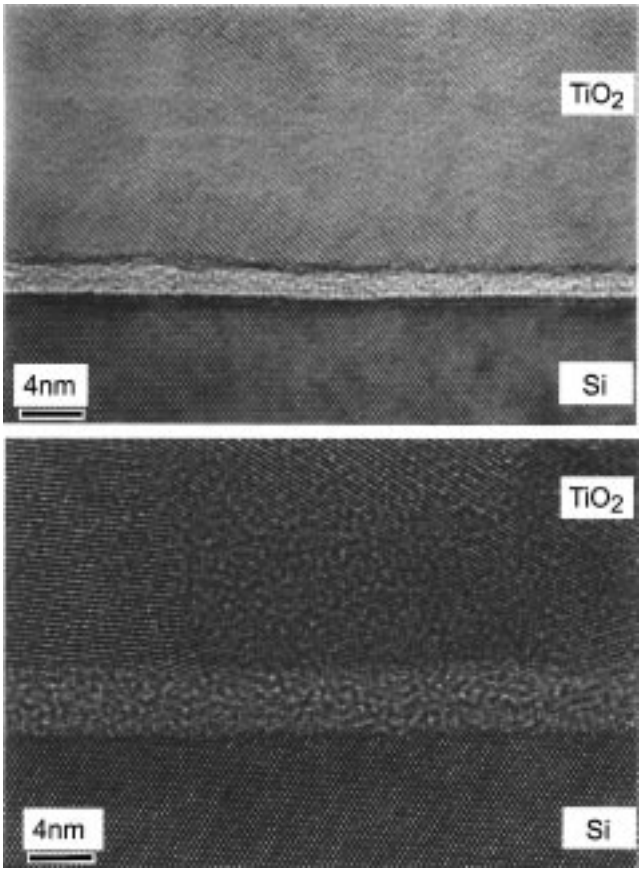

Figure 7. Cross-sectional TEM of TN (deposited at 280 °C) and TTIP-grown (deposited at 323 °C) films. Both micrographs show the amorphous interfacial layer.

surface collision rate (Z_P) and the precursor adsorption probability (S_P). If we assume that adsorption is well described by Langmuirian kinetics, then S_P may be expressed as the product of the zero coverage adsorption probability, $S_P°$, and the fraction of unoccupied precursor adsorption sites. Hence

$$\frac{d\Theta_P}{dt} = Z_P S_P° \left(\frac{\Theta_P° - \Theta_P}{\Theta_P°}\right) - k_{des}\Theta_P - k_r\Theta_P = 0 \quad (7)$$

where $\Theta_P°$ is the total number of sites available for precursor adsorption. From eq 7, we solve for Θ_P and then insert the result into eq 6, obtaining the following expression for the steady-state growth rate:

$$R = \frac{k_r Z_P S_P°}{(Z_P S_P°/\Theta_P°) + k_{des} + k_r} \quad (8)$$

The rate constants k_r and k_{des} can be expressed in simple Arrhenius form, i.e.

$$k = Ae^{-E_a/RT} \quad (9)$$

where A and E_a are the reaction frequency factor and activation energy, respectively. The zero coverage adsorption probability, $S_P°$, is often taken to be a temperature-independent quantity, and we do so in the kinetic modeling that we present below. We note, however, that Scoles and co-workers recently demonstrated that the physisorption probabilities of alkanes on gold decrease with increasing surface temperature.[42] The effect becomes especially pronounced above the characteristic alkane desorption temperature. Possible implications of a temperature-dependent adsorption probability for this work will be discussed below.

Table 3. Kinetic Parameters

param	TN	TTIP	param	TN	TTIP
$S°$	0.016	0.0032	E_{des} (kJ/mol)	140	240
E_r (kJ/mol)	100	135	A_{des} (s^{-1})	1.3×10^{12}	1.8×10^{14}
A_r (s^{-1})	1.2×10^{10}	3.5×10^{9}			

The expression in eq 8 is similar to one derived by Bent et al.[43] to analyze the kinetics of Al CVD using triisobutylaluminum, except that it allows for reversible precursor adsorption. By allowing for reversible adsorption, we are able to identify three (rather than two) limiting growth situations. In the first limiting situation, which pertains at low temperatures, the first term in the denominator is much larger than $k_{des} + k_r$, and the rate expression reduces to

$$R = k_r\Theta_P° \quad (10)$$

This corresponds to reaction-limited deposition kinetics. In this regime, the deposition rate is independent of precursor pressure, and the logarithm of the growth rate varies linearly with reciprocal temperature. From comparison of eqs 6 and 10, we note that, for a CVD process to be reaction-limited, the growth surface must be saturated with adsorbed precursor, because $\Theta_P = \Theta_P°$. When $k_r \gg k_{des} + (Z_P S_P°)$, the growth rate is independent of temperature and equal to $Z_P S_P°$. Growth is then rigorously flux-limited. The high-temperature limiting deposition occurs when $k_{des} \gg k_r + (Z_P S_P°)$. Now

$$R = \frac{k_r}{k_{des}} Z_P S_P° \quad (11)$$

Under these conditions, the growth rate is determined by the adsorption rate ($Z_P S_P°$) and the partitioning of the adsorbed precursor between the reaction and the desorption channels. Depending on the relative values of E_a for desorption and reaction, R can either increase or decrease with temperature. If the activation energy for desorption is greater than that for reaction, then k_{des} increases more rapidly with temperature than does k_r. The first term in eq 11 decreases with increasing temperature, and so does R. Thus, the observed trends in growth rate can be rationalized by invoking a mechanism in which the activation energy for precursor desorption is greater than that for reaction.

We fit the experimental growth rate data to the expression in eq 8. The values of Z_{TN} and Z_{TTIP} were calculated from gas-kinetic theory assuming a 25 °C gas. $\Theta_P°$ for both precursors was taken as the density (molecules·cm^{-2}) of TiO_2 units at the surface of single-crystal rutile. The linear growth rates were converted from units of nm·s^{-1} to molecules·cm^{-2}·s^{-1}, correcting for the film density. All other variables in eq 8 (i.e., A_r, E_r, A_{des}, E_{des}, and $S°$) were fitting parameters, the values of which are summarized in Table 3. Fitting of the data was made difficult by the fact that TiO_2 growth was never strictly reaction-limited under the conditions investigated in this work. For this reason, attempts to extract E_r and A_r directly from the data via linear regression analysis of the low-temperature growth rate points failed. Growth rates that were calculated using such parameters underpredicted the actual rates during the turnover from reaction- to flux-limited growth. Clearly, it would be desirable to

(42) Wetterer, S. M.; Lavrich, D. J.; Cummings, T.; Bernasek, S. L.; Scoles, G. *J. Phys. Chem. B* **1998**, *102*, 9266.

(43) Bent, B. E.; Nuzzo, R. G.; Dubois, L. H. *J. Am. Chem. Soc.* **1989**, *111*, 1634.

determine at least some of the rate parameters independently rather than rely on an unconstrained fit. We intend to carry out such studies soon.

In Figure 1 we compare the experimentally determined rate measurements with growth rate curves that were calculated from eq 8. Agreement between the fit and the data points is excellent. Although it is true that other combinations of rate parameters fit the data equally well, the goodness of the fit suggests that the kinetic model presented above captures the essence of the mechanism for TiO_2 growth from TN and TTIP. We note that the magnitudes of all rate parameters are physically reasonable, and that the activation energy for conversion of adsorbed TTIP to solid TiO_2 (135 kJ·mol^{-1}) is equal to that measured by other researchers using temperature-programmed desorption methods.[27]

From the kinetic fits, we conclude that the zero coverage adsorption probabilities of TN and TTIP are 0.016 and 0.0032, respectively. Although the uncertainties in $S_{TN}°$ and $S_{TTIP}°$ are significant (due to the fitting procedure and to the uncertainties of the precursor pressure measurements), it is safe to conclude that the $S°$ values are both much less than unity. The physical origin of such low $S°$ values is at present unknown, but one possibility is that the precursor adsorption sites are defects or step edges whose structure is such that they bind TN or TTIP more tightly than do other sites on the TiO_2 surface. The low $S°$ values may thus provide a key to understanding the precursor-specific film microstructures. If $S_{TN}°$ and $S_{TTIP}°$ were both close to unity, then one might expect the film microstructures to converge even in the reaction-limited regimes, because the growth surface could not distinguish between TN and TTIP. On the other hand, if TN and TTIP were to adsorb at different sites, it is easy to speculate that precursor-specific microstructures might develop.

Scoles and co-workers recently reported that the physisorption probabilities of alkanes on gold decrease with increasing surface temperature.[42] They attributed the effect, which is manifest only above the characteristic alkane desorption temperature, to inefficient accommodation of translational energy in the incoming alkane by the high-temperature surface. In the current study, a model invoking a temperature-independent value of $S°$ below 600 °C for TN or 700 °C for TTIP followed by an exponential temperature dependence at higher temperatures could also fit the data without recourse to a desorption step. Although these two schemes are kinetically indistinguishable, the requirement that $S°$ suddenly becomes temperature dependent at such high values seems unrealistic. In addition, we note that, for some systems, $S°$ does not depend on temperature.[44] Further experimental work is underway to clarify these issues.

Impact of Precursor Surface Diffusion. In addition to the adsorption, desorption, and reaction of the precursor discussed above, precursor diffusion (represented as k_{diff} in Scheme 1) will affect the microstructure. From eq 8, we see that reaction-limited and near-reaction-limited deposition kinetics imply a high steady-state coverage of adsorbed precursor. As an example, we show in Figure 8 how the estimated steady-state TTIP coverage ($\Theta_{\mathbf{P}} = R/k_r$) varies with temperature at a TTIP pressure of 4.0×10^{-5} Torr. (In Figure 8, we also compare the measured and calculated values of the absolute TiO_2 growth rates from TTIP.) Between 323 and 480 °C (roughly the low-temperature growth region of TTIP), the calculated precursor coverage varies between 94% and 5% of its maximum value. The high coverages result from the fact that the residence time

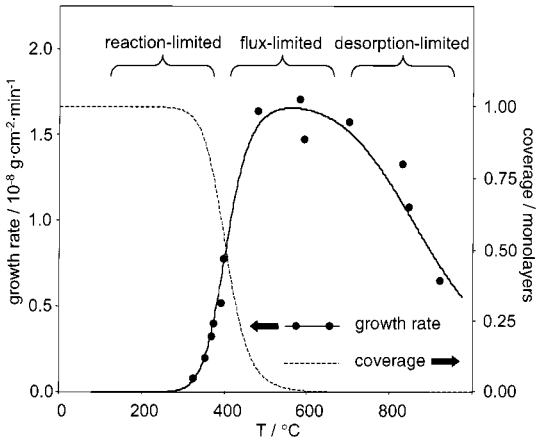

Figure 8. TTIP coverage and growth rate. The data points are from experimental measurements, and the solid (growth rate) and dashed (coverage) lines are derived from the model discussed in the text.

of an adsorbed precursor in this regime is long compared to the time between gas−surface collisions. The mean residence time, τ, of adsorbed **P** can be estimated from the fitting parameters:

$$\tau_{\mathbf{P}} = \frac{1}{k_r} + \frac{1}{k_{des}} \tag{12}$$

The value of τ decreases rapidly with increasing temperature. For TTIP, τ drops from ∼4 s at 400 °C (the midpoint of the reaction-limited regime) to 10^{-2} s at 600 °C (the temperature at which kinetics become clearly flux-limited).

As $\tau_{\mathbf{P}}$ increases, the distance the precursor can thermally diffuse across TiO_2 also increases. We have no information on the diffusion kinetics of TN or TTIP on TiO_2, but a useful rule of thumb is that the activation energy for diffusion of an adsorbed molecule is 15−30% of the desorption energy.[45] Focusing again on TTIP, we estimate the activation energy for diffusion as 60 kJ·mol^{-1} (25% of the desorption energy reported in Table 3), and we assume a value of 10^{10} s^{-1} for the diffusion prefactor. Under such conditions, the mean time between diffusive hops (ϑ) is 4.6×10^{-6} s at 400 °C and 3.9×10^{-7} s at 600 °C. A molecule of residence time τ will undergo τ/ϑ hops, on average, before reacting or desorbing. This number decreases with increasing temperature, from $\sim 2 \times 10^6$ for TTIP at 400 °C to $\sim 9 \times 10^4$ for TTIP at 600 °C. We thus see that, as temperature increases, the number of hops, and therefore the characteristic migration length, decreases. We note that although the calculated numbers may be in significant error, the trends are not. The residence time is controlled by the values of k_r and k_{des}, whereas ϑ is controlled by the diffusion rate constant. As the activation energies for reaction and desorption are almost certainly greater than those for surface diffusion, ϑ must increase more rapidly with temperature than τ, and so the characteristic migration length must decrease.

From the above analysis, we begin to see how the microstructure of a TiO_2 CVD film might be temperature- and precursor-specific. At low temperatures, the adsorbed precursors will sample a wide range of surface sites before reacting, as the characteristic reaction time is quite long. The diffusional path explored by an adsorbed molecule is a strong function of the adsorbate−surface potential energy surface. For TN and TTIP, which have very different structures, one might expect analogously different diffusional paths. For example, the nitrate

(44) Brown, D. E.; George, S. M.; Huang, C.; Wong, E. K. L.; Rider, K. S.; Smith, R. S.; Kay, B. D. *J. Phys. Chem.* **1996**, *100*, 4988.

(45) Seebauer, E. G.; Allen, C. E. *Prog. Surf. Sci.* **1995**, *49*, 265.

Scheme 2. Summary of Results from the Cross-Deposition Experiments: (A) TiO_2 Deposited on Silicon Using TN Followed by a Layer of TiO_2 Deposited Using TTIP, (B) Reversed Order of Precursor Use

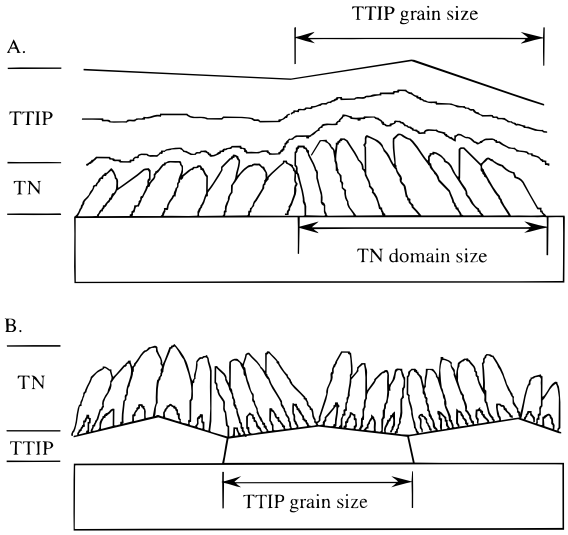

ligands on TN have lone electron pairs that could participate in specific donor−acceptor interactions with the TiO_2 surface, whereas the hydrocarbon nature of the TTIP ligands precludes such interactions. If the structure of the TiO_2 surface were highly anisotropic (as is the case for anatase and rutile), TN surface migration could be more rapid in some directions than in others, while TTIP migration could be isotropic. Under such conditions, one might predict equiaxed microcrystallites from TTIP and more unusually shaped crystallites from TN.

As temperature increases, the adsorbed precursors undergo fewer and fewer diffusional hops before reacting. Eventually, the characteristic migration length will become so short that the precursor will react at or desorb from the site on which it adsorbs. One would expect no influence of the precursor on film microstructure under such conditions, which is just what is observed for flux-limited TiO_2 deposition from TN and TTIP. At these higher temperatures diffusion of titanium and/or oxygen atoms (or ions) on a clean TiO_2 surface or along grain boundaries, represented by k'_{diff} in Scheme 1, will alter the microstructure. On the time scale of the depositions, the lack of sintering and grain growth at 500 °C establishes that the contribution of Ti and O diffusion at lower temperatures is minimal.

Cross-Deposition Studies. Scheme 2 outlines the results of the cross-deposition studies, which were conducted at temperatures where the difference in growth rates (and microstructures) was large (330 °C for TN and 374 °C for TTIP). The initial layer of TN-grown TiO_2 (Scheme 2A) would produce the usual pattern characteristic of this precursor (Figure 7). We observe that switching to TTIP results in evolution of a film whose final morphology is qualitatively similar to those of films deposited entirely from TTIP. The cross-deposition studies did produce TTIP-grown films with grain sizes larger than normally observed. Indeed the final grain size is the same as the domain size found in TN-grown films. Likewise the domain size of the TN-grown films deposited on the TTIP-grown TiO_2 is smaller than normally observed. As suggested in Scheme 2, the initial layer provides a template for growth of the second layer; however, at the thicknesses deposited in this study the final microstructure is still dominated by the characteristics of the precursor at that temperature.

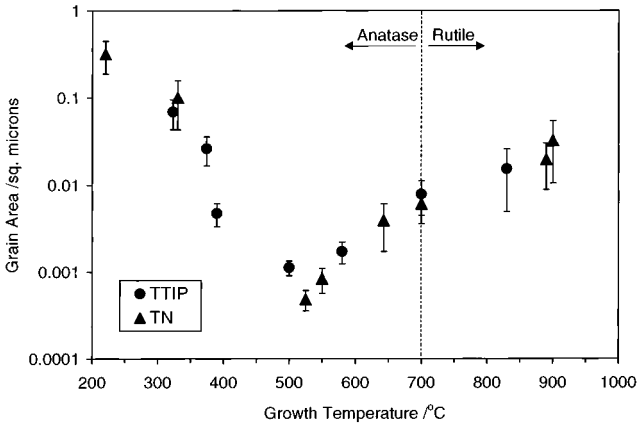

Figure 9. Semilog plot of grain size vs deposition temperature for both precursors. The error bars are shown at 1 standard deviation (Table 2). The vertical line at 700 °C shows the observed boundary between anatase (lower temperatures) and rutile.

In the temperature range around 350 °C where these cross-depositions were evaluated, $\tau_{TN} < \tau_{TTIP}$, and therefore, the distance that TTIP can diffuse is greater. This allows TTIP to fill in the gaps created in the TiO_2 films initially deposited from TN.

Reversing the order of the cross-deposition studies produces a film qualitatively similar to films deposited only from TN. As the TN molecules cannot diffuse as far before reacting, they deposit a larger number of subgrains on the TiO_2 surface. In addition, the microstructure of the TN-deposited films continues to reflect the anisotropy of TN diffusion (or reaction) on the TiO_2 surface.

Grain Size Trends and Anatase to Rutile Phase Transition. Figure 9 summarizes the temperature dependence of the grain size for both precursors. At temperatures above 500 °C, the grain sizes and shapes of TiO_2 grown from the two precursors are indistinguishable. As discussed previously, this is consistent with grain growth and sintering dominated by surface diffusion of the film constituents rather than the precursor. The trend of increasing grain size with increasing temperature is also consistent with this picture. Below 500 °C the trend of decreasing grain size with increasing temperature tracks the decreasing precursor lifetime on the surface.

The close agreement of the grain size (from TTIP) and the domain size (from TN) in the reaction rate-limited regime is remarkable. It would seem that despite radically different rate constants for reaction, desorption, and diffusion for TN and TTIP in this temperature regime, a common feature is determining the size of the grain/domain. More detailed evaluation of the crystallography and interface composition is aimed at answering this question. The TN-grown subgrains of TiO_2 are indeed much smaller than the grains deposited by TTIP.

On the basis of the standard heats of formation between 27 and 727 °C, the rutile phase is more stable than the anatase phase.[46] Despite this, at substrate temperatures below 650 °C, anatase is the only phase detected by XRD, an observation in agreement with published results on the formation of TiO_2 by many different solution- or gas-phase methods. This general observation has led to the proposal that the surface energy of anatase is lower than that of rutile such that at small grain sizes (<15 nm) anatase becomes more stable than rutile.[46−48]

In the current study, especially at lower temperatures, the grains are notably larger than 15 nm, yet anatase is still observed.

(46) Zhang, H. Z.; Banfield, J. F. *J. Mater. Chem.* **1998**, *8*, 2073.
(47) Gribb, A. A.; Banfield, J. F. *Am. Mineral.* **1997**, *82*, 717.
(48) Penn, R. L.; Banfield, J. F. *Am. Mineral.* **1998**, *83*, 1077.

On the basis of the classic picture of homogeneous nucleation, the same balance between bulk and surface energies that stabilizes anatase at small grain sizes creates a barrier to new phase formation. As this thermodynamic barrier increases, the rate of nucleation decreases and the number of grains becomes smaller. Providing sufficient precursor diffusion, those that form will reach larger grain sizes due to the reduced competition for precursor. On the basis of the argument that the surface energy of rutile is higher than that of anatase, we might also expect a higher thermodynamic barrier for the nucleation of rutile. Thus, anatase nucleates in preference to rutile, and as the nuclei will be smaller than 15 nm, there is no driving force to convert to rutile. These initial nuclei of anatase will act as a template for further growth, leading to larger grains of the same phase. The metastable anatase phase is retained even as the critical size for rutile formation is exceeded because the temperature is too low for the phase change to occur at a significant rate. Above 700 °C the rate of the anatase to rutile phase change is sufficient to produce films entirely of rutile.

Conclusions

Both TTIP and TN deposit high-quality, polycrystalline films of TiO_2. A two-step kinetic model involving reversible adsorption and irreversible reaction was found to fit the experimental results quantitatively over a very large temperature range. Comparison of the microstructures of films deposited at similar temperatures for TTIP and TN revealed significant differences in the reaction rate-limited regime. As the growth rates of the two precursors converged in the flux-limited regime, the respective microstructures became indistinguishable. In the reaction rate-limited regime the differences in microstructures were attributed to differences in the precursor lifetime on the surface, its characteristic diffusion length, and its selectivity. These effects also explain why the grain size of the TiO_2 decreased with increasing temperature for both precursors. At higher temperatures in the flux-limited regime and beyond, grain size increases with increasing temperature. In this regime microstructure is dominated by diffusion of titanium and/or oxygen atoms on the surface or along grain boundaries. This work suggests that the search for a dependence of film microstructure and properties on the structure of the molecular precursor should focus on the reaction rate-limited kinetic regime.

Acknowledgment. The authors gratefully acknowledge support from the Semiconductor Research Corporation.

JA984446F